Benchmarks of Multi-Component Signal Analysis Methods

Juan M. Miramont
IREENA
Nantes Université
Saint-Nazaire, France
ORCID:0000-0002-3847-7811
juan.miramont@univ-nantes.fr

Quentin Legros
LJK
University of Grenoble-Alpes
Grenoble, France
ORCID:0000-0003-1544-9655
legros.quentin2@hotmail.fr

Dominique Fourer
IBISC
Univ. Evry / Paris-Saclay
Evry-Courcouronnes, France
ORCID:0000-0002-7880-6261
dominique.fourer@univ-evry.fr

François Auger
IREENA
Nantes Université
Saint-Nazaire, France
ORCID:0000-0001-9158-1784
francois.auger@univ-nantes.fr

***Abstract*—Non-stationary multicomponent signals are ubiquitous in real-world applications. They can be modeled as a superimposition of amplitude- and frequency-modulated components so-called the modes, which require dedicated techniques to be efficiently analyzed and disentangled. State-of-the-art methods use specific assumptions and paradigms which can produce very different results in specific use cases. Hence, this paper aims to present and discuss the advantages and the limitations of several promising recent approaches respectively applied to signal denoising, mode retrieval and instantaneous frequency estimation through a comparative evaluation benchmark. Our numerical experiments show the specific scenarios where each method is the more adapted in terms of quality of mode separation and reconstruction while also considering the computational efficiency.**

***Index Terms*—non-stationary multicomponent signal, mode retrieval, comparative study, time-frequency, synchrosqueezing**

I. Introduction

Analyzing time series that comprise multiple oscillatory components with time-varying features, such as amplitude or frequency, is at the core of many applications in signal processing [1]–[3]. Problems of this nature can be addressed using the multicomponent signal (MCS) model, that can be expressed as

$$x(n) = \sum_{j=1}^{J} x_j(n), \text{ with } x_j(n) = a_j(n)\, \mathrm{e}^{i\phi_j(n)}, \qquad (1)$$

where $i^2 = -1$, $n \in \{0, 1, ..N-1\}$ is the time index, $x_j(n)$ is an AM-FM component or *mode*, $a_j(n)$ and $\phi_j(n)$ are, respectively, the instantaneous amplitude and phase functions of the j-th component and J is the number of components. A MCS analysis method can have different goals. Recovering the individual components $x_j(n)$ when $x(n)$ is contaminated with noise might be one of them, as well as estimating $a_j(n)$ and $\phi_j(n)$. In particular, one feature of the modes that applications are often interested in is the instantaneous frequency (IF), given by $\phi'_j(n) = \frac{\mathrm{d}\phi_j}{\mathrm{d}n}(n)$.

Time-frequency (TF) and time-scale representations are useful tools for analyzing MCS [4], allowing to reveal the time-varying frequency content of the signal and discern its components. We focus here on the Short-Time Fourier Transform (STFT) of a signal x, expressed as:

$$F_x^g(n,m) = \sum_{\ell=-\infty}^{+\infty} x(\ell) g(n-\ell)\, \mathrm{e}^{-i\frac{2\pi m \ell}{M}}, \qquad (2)$$

where $m \in \{0, 1, ..., M-1\}$ is the frequency bin and g is a real-valued analysis window.

The so-called *spectrogram* $S_x^g(n,m) = |F_x^g(n,m)|^2$ can then be interpreted as a TF energy distribution of the signal [4], [5]. Each mode in a MCS can be associated with local spectrogram maxima forming a *ridge*, a trajectory in the TF plane that approximately describes its IF. Detecting ridges is the cornerstone of a large number of MCS analysis methods, several promising ones [2], [6]–[8] are investigated in the remaining . Other methods might exploit the spectrogram zeros [9], [10], or even work in the time domain [11].

Since the choice of the suitable MCS analysis approach is not trivial for a given application scenario, this paper aims to compare several methods in three tasks: (1) Signal denoising, (2) Individual component reconstruction, and (3) IF estimation of each component. The aim of this work is twofold. First, we objectively discuss strengths and weaknesses of the explored approaches, so that future avenues of research can be identified. Second, we propose a common baseline to use in further research, that is easily accessible to all researchers. To this end, we use our previously proposed Python-based publicly-available toolbox for benchmarking that provides a framework for methods comparison for the sake of reproducibility and researcher independence [12].

The rest of the paper is organized as follows. Section II presents the main ideas of each investigated method in this comparative study. The comparative results obtained in the three considered tasks are presented in Section III and finally discussed in Section IV.

II. Methods

A. Synchrosqueezing Transform and Ridge Detection

The synchrosqueezing transform (SST) is a post-processing technique that yields sharper TF representations while allow-

This research was supported by the French ANR ASCETE project (ANR-19-CE48-0001)

ing reconstruction [13], [14]. It *vertically* reassigns the STFT coefficients according to $(n,m) \mapsto (n, \hat{\omega}_{(n,m)})$, such as

$$\mathcal{T}_x(n,m) = \sum_{q:|m-\hat{\omega}(n,q))|\leq 1/2} F_x^g(n,q)\, \mathrm{e}^{i\frac{2\pi qn}{M}} \quad (3)$$

where $\hat{\omega}(n,m) = m - \frac{M}{2\pi}\Im\left\{\frac{F_x^{g'}(n,m)}{F_x^g(n,m)}\right\}$, $F_x^g(n,m) \neq 0$, estimates the IF of the signal component located at (n,m). When combined with a ridge detection (RD) algorithm [15], the synchrosqueezed STFT allows to individually retrieve the signal components as:

$$\tilde{x}_j(n) = \frac{1}{Mg(0)} \sum_{q\in\left[\hat{\Omega}_j(n)-\epsilon/2,\hat{\Omega}_j(n)+\epsilon/2\right]} \mathcal{T}_x(n,q), \quad (4)$$

where $\hat{\Omega}_j(n)$ is the estimated ridge corresponding to the j-th mode, and $\epsilon > 0$ is the width of a strip around the ridge. For this method, we use the RD method first proposed by Brevdo et al. in [16], [17], which estimates the best $\Omega_j(n)$ as

$$\hat{\Omega}_{j(n)} = \arg\max_{\Omega_j} \sum_{n=0}^{N-1} |\mathcal{T}_x(n,\Omega_{j(n)})|^2 - \lambda \sum_{n=0}^{N-2} |\Delta\Omega_{j(n)}|^2 \quad (5)$$

where $\Delta\Omega_j(n) = \Omega_j(n+1) - \Omega_j(n)$ and λ controls the smoothness of the solution. After removing the energy associated with $\hat{\Omega}_j(n)$ from $\mathcal{T}_x(n,m)$, $\hat{\Omega}_{j+1}(n)$ can be found by solving again (5), repeating this process up to the J-th ridge in a so-called *peeling* scheme. In the following, we refer to this method as *SST+RD*.

B. Modulation-Based Ridge Detection

In [6], the authors propose to improve the Brevdo's method by introducing a modulation-based RD (MB-RD) approach. There, the ridges are estimated as:

$$\hat{\Omega}_j(n) = \arg\max_{\Omega_j} \sum_{n=0}^{N-1} |F_x^g(n,\Omega_k(n))|^2, \quad \text{s.t.}\, |\Delta\Omega_j(n) - M\hat{q}(n,\Omega_j(n))| < C \quad (6)$$

where $\hat{q}(n,m)$ is the real part of the complex modulation operator used in second order SST [18], which is an estimator of $\phi_j''(n)$. Two mode reconstruction strategies are used here along with MB-RD: 1) Simple Reconstruction (SR): considering STFT coefficients in a neighborhood of the detected ridge that are above a given noise threshold [2], [6], and 2) Local Linear Chirp (LCR) approximation of the mode, described in [2], [19].

C. Pseudo-Bayesian ridge detection

The pseudo-Bayesian (PB) method [7] addresses the IF estimation problem, by detecting the ridges on the TF plane within a Bayesian framework. The spectrogram of the observed signal is modeled as a random variable assuming the presence of a unique component at each TF point, as:

$$s_{n,m}|\phi'(n) \sim h\left(m - \phi'(n)\right) \quad (7)$$

with $h(m) = e^{-\left(\frac{2\pi mL}{M}\right)^2}$, L being a parameter related to the time spread of the analysis window g. The Bayesian model is completed by assigning to $\phi'(n)$ a Gaussian random walk prior model to enforces spatial smoothness. Instead of the classical Kullback–Leibler cross entropy, an alternative divergence [20] is minimized to account for the lack of generality of the model. While sequential moment matching performed over the time axis provides a single ridge estimate, the method is repeated for each component after removal of the spectrogram energy in a neighborhood of the detected ridge [21].

D. Stochastic Expectation Maximization

The Bayesian method proposed in [8] performs IF and amplitude estimation of multicomponent signals whose modes can overlap in the TF plane. The observed signal spectrogram is modeled as a mixture $p(s_{n,m}|\boldsymbol{w}_n, \boldsymbol{\phi'}_n) =$

$$\sum_{j=1}^{J} w_{n,j} h(m - \phi_j'(n)) + \frac{1}{M}\left(1 - \sum_{j=1}^{J} w_{n,j}\right), \quad (8)$$

with $\boldsymbol{w}_n = [w_{n,1}, \ldots, w_{n,J}]^\top$ the mixture weights at time instant n, and $\boldsymbol{\phi'}_n = [\phi_1'(n), \ldots, \phi_J'(n)]^\top$. A stochastic Expectation Maximization (SEM) algorithm [22] is used to estimate the model parameters. It consists in iteratively approximating the prior models using a Markov Chain Monte Carlo approach, followed by the classical steps of the EM algorithm

$$\begin{aligned} Q(\boldsymbol{\mathcal{W}}|\boldsymbol{\mathcal{W}}^{(i)}) &= E_{\boldsymbol{\Phi'}|\boldsymbol{\mathcal{W}}^{(i)},\boldsymbol{S}}\left[\log(p(\boldsymbol{\mathcal{W}}, \boldsymbol{\Phi'}|\boldsymbol{S}))\right] \\ \boldsymbol{\mathcal{W}}^{(i+1)} &= \underset{\boldsymbol{\mathcal{W}}}{\operatorname{argmax}}\ \ Q(\boldsymbol{\mathcal{W}}|\boldsymbol{\mathcal{W}}^{(i)}), \end{aligned} \quad (9)$$

with with $\boldsymbol{S} = \{\boldsymbol{s}_n\}_{n=0}^{N-1}$ such as $\boldsymbol{s}_n = [s_{n,0}, \ldots, s_{n,M-1}]^\top$, and $\boldsymbol{\mathcal{W}}^{(i)}$ the current estimation of $\boldsymbol{\mathcal{W}}$ at iteration i, $\boldsymbol{\mathcal{W}} = \{\boldsymbol{w}_n\}_{n=0}^{N-1}$ and $\boldsymbol{\Phi'} = \{\boldsymbol{\phi'}_n\}_{n=0}^{N-1}$. A post-processing step interpolates the estimated IF in overlapping regions.

E. Finite Rate of Innovation

In [23], a mode estimation method based on a sparse modeling of the signal innovation is proposed. The signal spectrogram vertical slices are modeled as

$$s_{n,m} \approx \sum_{j=1}^{J} a_j^2(n)\, h(m - \phi_j'(n)) \quad (10)$$

which is assumed to be the convolution between a stream of Dirac of weight $a_k^2(n)$ and located at $\phi_k'(n)$, with the window h. The signal modes are estimated by reconstructing the stream of Dirac pulses $f_n(m) = \sum_j a_j^2(m)\delta(m - \phi_j'(n))$, using the finite rate of innovation principle [24], [25]. From Eq. (10), we have

$$s_{n,m} = \sum_{q=-\infty}^{\infty} F_h(q) \underbrace{\sum_{j=1}^{J} a_j^2(n)\, \mathrm{e}^{\frac{-i2\pi q\phi_j'(n)}{M}}}_{F_{f_n}(q)} \mathrm{e}^{\frac{i2\pi qm}{M}} \quad (11)$$

with F_h (resp. F_{f_n}) the discrete Fourier transform of h (resp. f_n). An alternative to the Prony method is then used

to estimate $\phi'_j(n)$ from f_n. Authors indeed resort to a total least squared approach (TLS) [25] to avoid model mismatch. It consists in replacing the annihilating filter by the minimizer of $\|\boldsymbol{A}\boldsymbol{h}\|^2, \text{s.t.} \|\boldsymbol{h}\|^2 = 1$. In the following, we refer to this approach as FRI method.

F. Delaunay Triangulation of the Spectrogram Zeros

As shown in [9], the zeros of the spectrogram can be used to identify the TF signal domain, allowing to disentangle signal and noise. Indeed, the zeros of the spectrogram of white Gaussian noise (WGN) are uniformly distributed in the TF plane [9], a phenomena that is mathematically described in detail in [10]. When a signal is present, the distribution of the spectrogram zeros is disrupted, and large regions without zeros are generated, corresponding to the TF domain of the signal. Then, one can estimate these regions by computing a Delaunay triangulation (DT) of the zeros of the spectrogram, and selecting the triangles with at least one edge longer than a previously fixed threshold $e_{\max}$ [9]. We shall use here two empirically chosen values of $e_{\max} = 1.45$ and $e_{\max} = 1.75$. Finally only the J more energetic components are extracted. Because this method is not based on RD, we estimate the IF as the finite difference approximation of the derivative of the phase of the complex-valued component $z_j(n)$, obtained by inverting $F_x^g(n,m)$ considering only the upper-half of the TF plane, previous multiplication with a binary extraction mask of the j-th component.

III. Numerical Results

In this section, we report and discuss the results of the proposed benchmarks. In order to compare the investigated methods, we used a freely-available, Python-based, benchmarking toolbox [12] that allows to compare methods implemented in Matlab or in Python. This approach gives interested readers the chance to easily download the benchmarks and to include their own methods to compare them with the ones used in this work (instructions are given in the benchmark public repository)[1]. The benchmark configuration requires defining a set of signals to use (from more than 20 signals offered by the toolbox), a range of SNRs to explore (using additive real WGN in this case), and choosing a performance metric. For the denoising and component retrieval benchmarks, this metric is the so-called quality reconstruction factor (QRF): $\text{QRF}(z,\hat{z}) = 10\log_{10}(\|z\|^2/\|z-\hat{z}\|^2)$, where z is the noiseless signal (or component), $\hat{z}$ is an estimation of z, and $\|\cdot\|$ is the usual 2-norm. For the IF estimation performance we use the mean squared error (MSE): $\text{MSE}(z,\hat{z}) = \frac{1}{N}\sum_{q=0}^{N-1}(z-\hat{z})^2$, where $\hat{z}$ is the IF estimation and z is the true IF. Fig. 1 shows the spectrograms of the synthetic signals used in the three benchmarks, with $N = 1024$, for SNRs ranging from -20 to 20 dB, in steps of 10 dB.

[1]Codes available at: https://github.com/jmiramont/benchmarks_eusipco2023

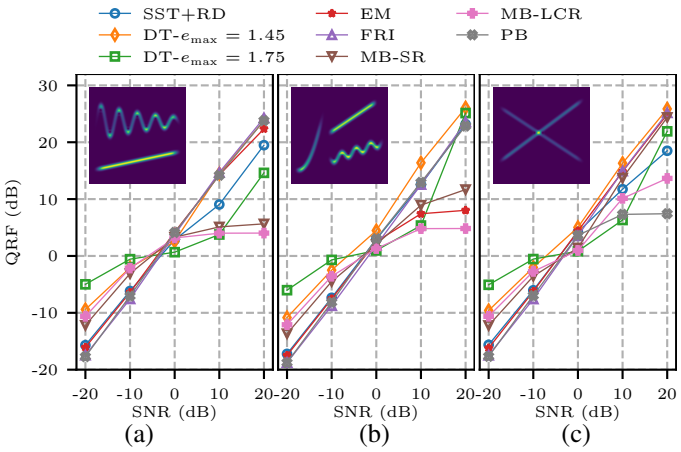

Fig. 1. Signal denoising results given as the average QRF over 30 realizations. The spectrogram of the synthetic signal is shown in each plot for reference.

A. Signal Denoising

Fig. 1 shows the signal denoising results of three MCSs, the spectrogram of which are shown in each subfigure. For high SNR, the most competitive methods are DT (with $e_{\max} = 1.45$), followed by PB, FRI and EM. For low SNR, the best method was DT (with $e_{\max} = 1.75$), whereas DT (with $e_{\max} = 1.45$) MB-SR and MB-LCR showed a comparable performance. Because DT behaves essentially as a hard-threshold approach, given that large regions without zeros in the plane coincide with those with high energy, a strict threshold $e_{\max} = 1.75$ provides the best results for SNR < 0 dB, whereas $e_{\max} = 1.45$ is more appropriate for SNR > 0 dB. Some methods can experiment difficulties when the components do not last the entire duration of the signal, as shown in Fig. 2b, where PB, FRI and EM perform worst than with the signal used in Fig. 2a.

B. Signal Components Estimation

Figs. 2a and 2b show the QRF of the reconstructed components of the signal used in Fig. 1a. This signal has two components: a sinusoidal chirp (the spectrogram of which is shown for reference in Fig. 2a), and a linear chirp (Fig. 2b). We stress that all methods receive the entire signal, consisting in the sum of both components. As before, DT ($e_{\max} = 1.45$ and $e_{\max} = 1.75$) shows the best performance for low SNR, followed by MB-LCR and MB-LCR for both components. For higher SNR, FRI and PB are the methods with the best performance for the more challenging sinusoidal chirp, followed by EM and DT (with $e_{\max} = 1.45$). In the case of the linear chirp, however, the more competitive methods are MB-SR and DT.

C. Instantaneous Frequency Estimation

Figs. 2c and 2d show the MSE of the IF estimation for the individual components of the signal shown in Fig. 1a. These results show how an effective IF estimation does not necessary imply a satisfactory reconstruction of the individual

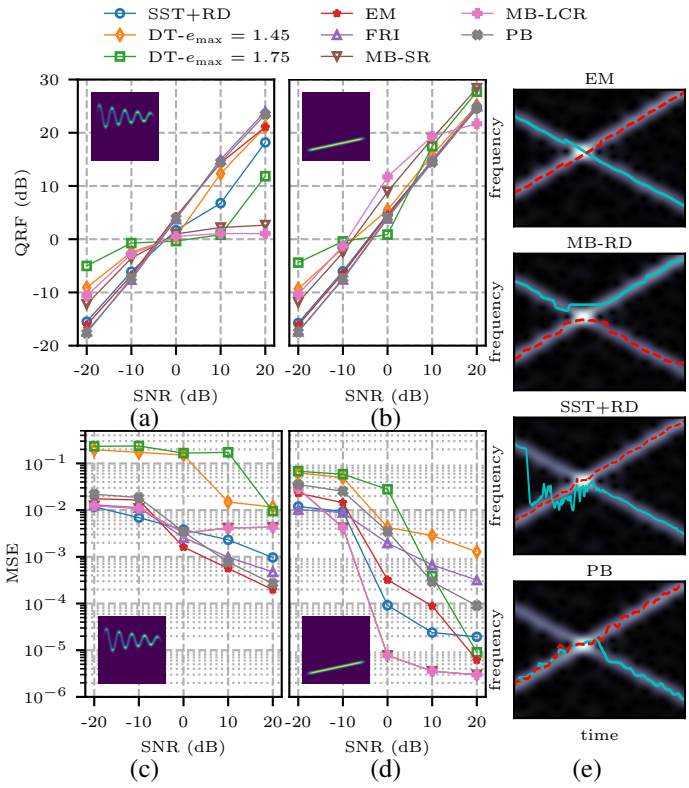

Fig. 2. (a) and (b): Quality reconstruction factor (QRF) of the individual components of the signal displayed in Fig. 1a. (c) and (d): Mean squared error (MSE) of the IF estimation for the same signal. The spectrogram of the analyzed component is shown in each plot for reference. The results shown (QRF and MSE) are the average of over 30 realizations. MB-SR and MB-LCR are superimposed because they both use RD-MB. (e) IF estimations of the crossing chirps in the signal shown in Fig. 1c. The estimations are superimposed to the spectrogram of the signal near the crossing point.

components, and vice versa. For instance, even though DT provides the best results in terms of the QRF for low SNR, this does not result in a better estimation of the IF (see Fig. 2c). In contrast, ridge-based methods, being naturally suited for this task, perform better. Considering the sinusoidal chirp, Fig. 2c, EM provided the best IF estimation for SNR ≥ 0 dB. For lower SNRs, SST+RD and MB-RD were the most competitive methods. However, MB-RD was the most effective method considering the linear chirp component, Fig. 2d, although FRI and SST+RD resulted in the best IF estimation for SNR $= -20$ dB.

Let us consider now the signal with overlapping chirps from Fig. 1c. Fig. 2e shows the IF estimations obtained with different methods, superimposed to the spectrogram. The top panel shows that EM results in more smooth approximations of the IF that correctly separates both chirps at the crossing point.

D. Computational Complexity

Here we assess the computational complexity of the competing methods by comparing their computational time, expressed in seconds, in diverse scenarios. More precisely, the computational efficiency of the methods is evaluated according to the number of frequency bins M and signal length N. The results obtained with $N = 512$ (resp. $N = 1024$) are presented in Table I. All the experiments were run on an Intel CORE i9 with 32 GB of RAM using Matlab 2022a and Python 3.9. The fastest methods were SST+RD, MB-RD and PB, while the slowest method was found to be EM by at least two orders of magnitude. However, as seen before, the latter can provide better IF estimations than other methods. The large computational complexity of the EM method is mainly due to the likelihood computation, performed at each iteration of the algorithm.

TABLE I
COMPUTATION TIME FOR A SIGNAL WITH $J = 2$ COMPONENTS, SNR $= 10$ DB, AND LENGTH $N \in \{512, 1024\}$. QRF IS IN DB. THE COMPUTATION TIME IS GIVEN IN SECONDS. THE BEST RESULTS PER COLUMN ARE BOLDFACED.

Method		$M = 512$	$M = 1024$	$M = 2048$
SST+RD	mean QRF	12.55	11.78	9.29
	comp. time	**0.12**	**0.21**	**0.41**
EM	mean QRF	12.39	11.87	8.36
	comp. time	5.16	36.23	133.01
DT	mean QRF	**13.29**	11.81	4.39
	comp. time	0.40	0.63	1.08
FRI	mean QRF	11.91	**12.91**	**11.93**
	comp. time	0.29	0.40	0.71
PB	mean QRF	13.02	9.88	10.09
	comp. time	0.27	0.27	0.29
MB-RD	mean QRF	11.06	11.25	11.22
	comp. time	0.18	0.26	**0.41**

(a) $N = 512$.

Method		$M = 512$	$M = 1024$	$M = 2048$
SST+RD	mean QRF	13.66	13.79	13.36
	comp. time	**0.23**	**0.43**	0.85
EM	mean QRF	14.45	14.61	**14.69**
	comp. time	10.19	72.21	256.23
DT	mean QRF	**14.68**	**15.03**	14.59
	comp. time	0.80	1.27	2.17
FRI	mean QRF	11.82	11.83	11.79
	comp. time	0.60	0.90	1.41
PB	mean QRF	12.99	14.75	11.60
	comp. time	0.88	0.96	1.07
MB-RD	mean QRF	11.60	11.51	11.08
	comp. time	0.36	0.53	**0.83**

(b) $N = 1024$.

E. Examples With a Real-World Signal

In this section, we evaluate the behavior of the methods on a real-world signal[2], whose spectrogram is displayed in Fig. 3a. The IF estimation of three modes performed using the EM, MB-RD and PB method, are respectively displayed in Fig. 3b, 3c and 3d. According to Fig. 3, all the methods estimate the three main components (with highest energy). MB-RD, EM and PB obtain mostly similar satisfying results for the IF curves of the three main components.

Figs. 3e and 3f show the mask obtained with DT using $e_{\max} = 1.45$ and $e_{\max} = 1.75$ respectively. Despite obtaining

[2]The authors wish to thank Curtis Condon, Ken White, and Al Feng of the Beckman Institute of the University of Illinois for the bat signal data and for permission to use it in this paper.

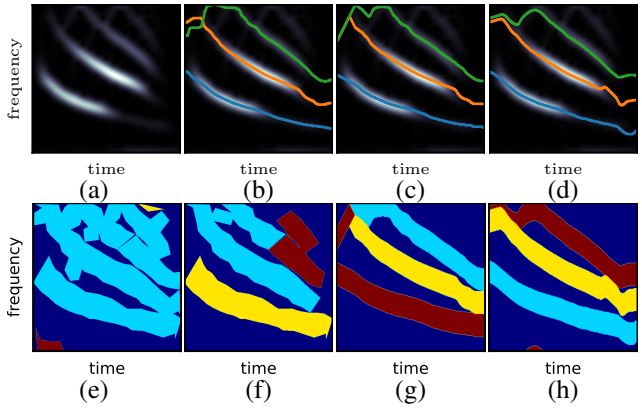

Fig. 3. First row: IF estimations (in colored lines) superimposed to the spectrogram of a bat echolocation signal. (a) Spectrogram of the signal (for reference). (b) IF estimation using MB-RD method. (c) IF estimation using EM method. (d) IF estimation using PB method. Second row: binary extraction masks for three methods. Different colors indicate the different extracted components. (e) DT method with $e_{\max} = 1.45$. (f) DT method with $e_{\max} = 1.75$. (g) EM method. (h) PB method.

more complete extraction masks than with other approaches, the estimated components in this case can be mixtures of the original ones, as can be seen from the colors in the masks shown in the figures. In contrast, RD-based, EM and FRI methods can discriminate between closer components more effectively, as long as the ridges can be detected [26].

IV. Conclusions

We compared several recently-proposed MCS analysis methods for three tasks: signal denoising, component retrieval and IF estimation. For the first task, DT obtained the best results, although the performance is highly dependent on the selected threshold $e_{\max}$. FRI, PB and MB-SR showed comparable results for high SNR, whereas for low SNR, MB-LCR and MB-SR were more competitive. DT can adapt to a wide variety of signal domain shapes, which makes it more appealing for cases with strong amplitude modulation.

Considering individual component reconstruction, PB, MB-SR and DT ($e_{\max} = 1.45$) yielded the best results for high SNR. For IF estimation however, the best approaches were MB-RD and EM, although for very low SNRs, FRI and SST+RD are more suitable choices. Future work will focus on strategies to automatically determine the optimal hyper-parameters of each method, such as the value of $e_{\max}$ used in DT. Reducing the computational cost of the EM method also remains an open issue. Furthermore, it could be interesting to extend this benchmark by investigating more methods, especially the new ones proposed in the future.

References

[1] H.-T. Wu, "Current state of nonlinear-type time–frequency analysis and applications to high-frequency biomedical signals," *Current Opinion in Systems Biology*, vol. 23, pp. 8–21, 2020.

[2] N. Laurent and S. Meignen, "A novel ridge detector for nonstationary multicomponent signals: Development and application to robust mode retrieval," *IEEE Transactions on Signal Processing*, vol. 69, pp. 3325–3336, 2021.

[3] K. Abratkiewicz and J. Gambrych, "Real-time variants of vertical synchrosqueezing: Application to radar remote sensing," *IEEE Journal of Selected Topics in Applied Earth Observations and Remote Sensing*, vol. 15, pp. 1760–1774, 2022.

[4] P. Flandrin, *Time-frequency/time-scale analysis*. Academic press, 1998.

[5] L. Cohen, "Generalized phase-space distribution functions," *Journal of Mathematical Physics*, vol. 7, no. 5, pp. 781–786, 1966.

[6] M. A. Colominas, S. Meignen, and D.-H. Pham, "Fully adaptive ridge detection based on STFT phase information," *IEEE Signal Processing Letters*, vol. 27, pp. 620–624, 2020.

[7] Q. Legros and D. Fourer, "Pseudo-Bayesian approach for robust mode detection and extraction based on the STFT," *Sensors*, vol. 23, no. 1, p. 85, 2022.

[8] Q. Legros, D. Fourer, S. Meignen, and M. A. Colominas, "Instantaneous frequency estimation in multi-component signals using stochastic EM algorithm," *arXiv preprint arXiv:2203.16334*, 2022.

[9] P. Flandrin, "Time–frequency filtering based on spectrogram zeros," *IEEE Signal Processing Letters*, vol. 22, no. 11, pp. 2137–2141, 2015.

[10] R. Bardenet, J. Flamant, and P. Chainais, "On the zeros of the spectrogram of white noise," *Applied and Computational Harmonic Analysis*, vol. 48, no. 2, pp. 682–705, 2020.

[11] J. Harmouche, D. Fourer, F. Auger, P. Borgnat, and P. Flandrin, "The sliding singular spectrum analysis: A data-driven nonstationary signal decomposition tool," *IEEE Transactions on Signal Processing*, vol. 66, no. 1, pp. 251–263, 2017.

[12] J. Miramont, R. Bardenet, P. Chainais, and F. Auger, "A public benchmark for denoising and detection methods," in *XXVIII Colloque Francophone de Traitement du Signal et des Images (GRETSI), Nancy, France, September 06–09, 2022*, Nancy, France, 2022.

[13] I. Daubechies and S. Maes, "A nonlinear squeezing of the continuous wavelet transform based on auditory nerve models," in *Wavelets in medicine and biology*. Routledge, 2017, pp. 527–546.

[14] I. Daubechies, J. Lu, and H.-T. Wu, "Synchrosqueezed wavelet transforms: An empirical mode decomposition-like tool," *Applied and computational harmonic analysis*, vol. 30, no. 2, pp. 243–261, 2011.

[15] R. A. Carmona, W. L. Hwang, and B. Torrésani, "Multiridge detection and time-frequency reconstruction," *IEEE transactions on signal processing*, vol. 47, no. 2, pp. 480–492, 1999.

[16] E. Brevdo, N. S. Fuckar, G. Thakur, and H.-T. Wu, "The synchrosqueezing algorithm: a robust analysis tool for signals with time-varying spectrum," *arXiv preprint arXiv:1105.0010*, 2011.

[17] G. Thakur, E. Brevdo, N. S. Fučkar, and H.-T. Wu, "The synchrosqueezing algorithm for time-varying spectral analysis: Robustness properties and new paleoclimate applications," *Signal Processing*, vol. 93, no. 5, pp. 1079–1094, 2013.

[18] D.-H. Pham and S. Meignen, "High-order synchrosqueezing transform for multicomponent signals analysis—with an application to gravitational-wave signal," *IEEE Transactions on Signal Processing*, vol. 65, no. 12, pp. 3168–3178, 2017.

[19] N. Laurent and S. Meignen, "A novel time-frequency technique for mode retrieval based on linear chirp approximation," *IEEE Signal Processing Letters*, vol. 27, pp. 935–939, 2020.

[20] F. Futami, I. Sato, and M. Sugiyama, "Variational inference based on robust divergences," in *Proc. Intern. Conf. on Artificial Intel. and Stat.*, A. J. Storkey and F. Pérez-Cruz, Eds., vol. 84. Playa Blanca, Lanzarote, Canary Islands, Spain: PMLR, 2018, pp. 813–822.

[21] Q. Legros and D. Fourer, "A novel pseudo-bayesian approach for robust multi-ridge detection and mode retrieval," in *29th European Signal Processing Conference (EUSIPCO)*, 2021, pp. 1925–1929.

[22] G. McLachlan and T. Krishnan, *The EM algorithm and extensions*. John Wiley & Sons, 2007, vol. 382.

[23] Q. Legros and D. Fourer, "Time-frequency ridge estimation of multi-component signals using sparse modeling of signal innovation," *arXiv preprint arXiv:2212.11343*, 2022.

[24] M. Vetterli, P. Marziliano, and T. Blu, "Sampling signals with finite rate of innovation," *IEEE Transactions on Signal Processing*, vol. 50, no. 6, pp. 1417–1428, 2002.

[25] T. Blu, P.-L. Dragotti, M. Vetterli, P. Marziliano, and L. Coulot, "Sparse sampling of signal innovations," *IEEE Signal Processing Magazine*, vol. 25, no. 2, pp. 31–40, 2008.

[26] N. Delprat, "Global frequency modulation laws extraction from the Gabor transform of a signal: A first study of the interacting components case," *IEEE Transactions on Speech and Audio Processing*, vol. 5, no. 1, pp. 64–71, 1997.